Material Distribution across the Interface of Random and Ordered Island Arrays

G. S. Kar,* S. Kiravittaya, M. Stoffel, and O. G. Schmidt

Max-Planck-Institut für Festkörperforschung, Heisenbergstrasse 1, D-70569 Stuttgart, Germany

(Received 2 July 2004; published 7 December 2004)

We grow single and twofold stacked island layers on patterned substrates and investigate the material distribution in and around the patterned area. For both layers a pronounced material depletion region occurs outside the pattern. The material gradients across the planar-patterned interface are symmetric in the first, but highly asymmetric in the second layer. We can describe these phenomena by simulations that take into account the surface curvature for the first and a strain-field modulated surface for the second layer.

DOI: 10.1103/PhysRevLett.93.246103 PACS numbers: 68.65.Hb, 68.35.Md, 81.07.Ta, 81.15.Hi

It is foreseeable that the full potential of self-assembled quantum dots [1] can be unleashed only if a controlled positioning and high integration of these nanostructures inside more complex device architectures can be realized. For this purpose people have grown self-assembled islands on patterned substrates, where the formation sites could be rigorously controlled [2,3]. The ability to laterally align self-assembled islands into dense periodic arrays has opened the path to investigate novel growth phenomena [4–7] as well as to fabricate quantum dot arrays with excellent size homogeneity [3,8].

In this Letter, we investigate the distribution of material accommodated in self-assembled islands across the interface of random and ordered island arrays in both single and twofold stacked layers. A pronounced island-free region around the patterned area is measured in both layers, which we interpret as a material depletion region. From the material distribution across the interface, we deduce a symmetric diffusion process in the first, but a highly asymmetric diffusion process in the second layer. The observed results can be explained by a growth model that considers the patterned area in the first layer as a simple material "sink" but needs to take into account the strain fields originating from buried islands in the case of the second layer.

We fabricated patterned areas ($60 \times 50\ \mu m^2$) by standard electron-beam lithography and reactive ion etching on Si(001) substrates. Each patterned field consists of trenches having a depth of 24 nm, a width of 120 nm, and a period of 320 nm. After patterning, the substrate was transferred into a solid source molecular beam epitaxy chamber and a 50 nm Si buffer layer was grown at 0.1 nm/s, while the substrate temperature was increased from 460 to 620 °C. All subsequent layers were grown at 620 °C. Then, 5 or 7 monolayers (MLs) of Ge were deposited at a growth rate of 0.044 ML/s for the single layer samples. For the twofold stacked layer samples, the initial 7 ML Ge island layer was overgrown with 30 nm Si and a second (4 or 7 ML thick) Ge layer was grown on a flat surface. Under these conditions, a perfect vertical alignment of Ge islands was observed [9]. The island morphologies were investigated *ex situ* by a Nanoscope IIIa atomic force microscope (AFM) in tapping mode.

In Fig. 1(a) we show a large AFM image ($80 \times 80\ \mu m^2$) obtained after deposition of 5 ML Ge on the whole surface area. The patterned area ($60 \times 50\ \mu m^2$) can be recognized in the center of the AFM image. Although we cannot resolve individual islands from this large area scan, we can nevertheless identify an island-free region surrounding the patterned area, which we interpret as a material depletion region [10]. This region, which is bordered by randomly distributed islands on the flat surface, is observed independently of the Ge coverage (5–7 ML).

In order to obtain a more detailed picture of the surface morphology, we took ($5 \times 5\ \mu m^2$) AFM scans along the path indicated in Fig. 1(a). One-dimensional chains of well-aligned Ge islands are clearly observed in the predefined patterned trenches [Figs. 1(b) and 1(c)] as has been reported previously [6,11], while a random island distribution is evident on the flat surface surrounding the patterned area [Figs. 1(d) and 1(e)]. On the flat surface, the islands consist of a bimodal distribution of pyramids (density: 5.3 μm^{-2}) and domes (density: 4.1 μm^{-2}). At the center of the patterned area, we observe mainly pyramid islands, while dome islands are located predominantly near the inner edge of the pattern. It is well known that during growth at a constant temperature a transition from pyramids to domes occurs when the Ge coverage increases [12,13]. Since the island density within the patterned area stays constant at $12.6 \pm 0.7\ \mu m^{-2}$, our results directly imply that more Ge adatoms accumulate near the inner edge than in the middle of the pattern. This observation together with the material depletion region around the patterned area indicates that a directional diffusion occurs from the unpatterned, flat surface towards the patterned area. In order to quantify the material distribution across the interface, we determine the total material accommodated in the islands per unit area, Θ, from a series of AFM scans taken across the center of the patterned area. The results are summarized in Fig. 2(a) for the first and in Fig. 2(b) for the second island layer.

 © 2004 The American Physical Society

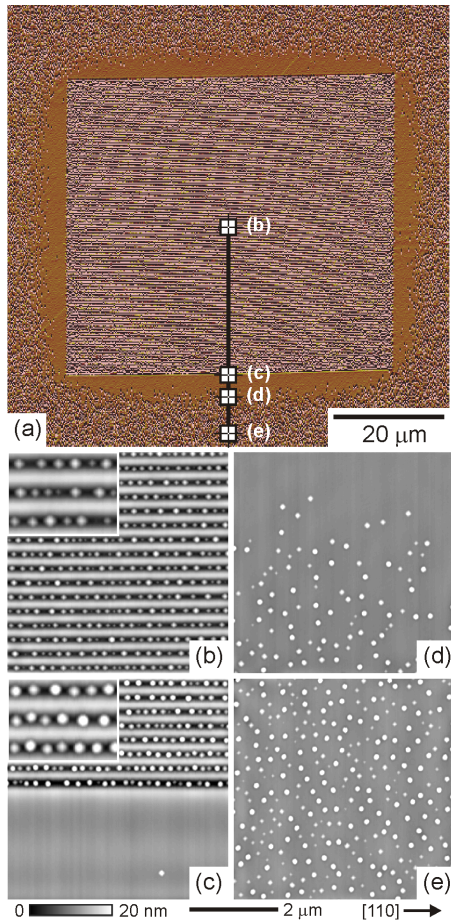

FIG. 1 (color online). (a) Large area (80×80 μm^2) AFM image of a single 5 ML Ge island layer sample (620 °C) with the patterned area in the center of the image. (b)–(e) AFM images (5×5 μm^2) of the areas marked in (a). An island-free region is clearly observed around the pattern. The insets of (b) and (c) are zoomed AFM images (1.2×0.9 μm^2).

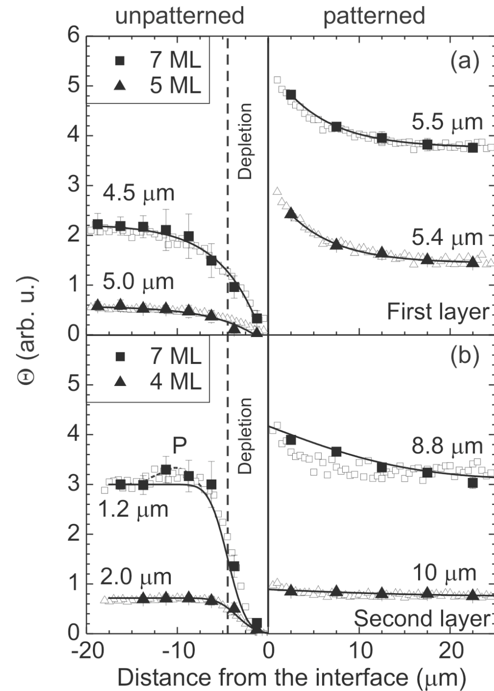

FIG. 2. Distribution of total material accommodated in the islands per unit area (Θ) across the interface for (a) the first layer with 5 (▲) and 7 (■) ML Ge deposition and (b) the second layer with 4 (▲) and 7 (■) ML Ge deposition. The simulation results (open symbols) are presented along with experimental results. The solid lines correspond to fits of the experimental data. Diffusion lengths are also indicated.

First we consider the case of a single island layer [Fig. 2(a)]. For 5 and 7 ML Ge depositions, Θ increases when moving from the center of the patterned area towards the interface and it decreases when moving from the unpatterned area towards the interface. The experimental results (solid symbols) were fitted (solid lines) using a simple exponential function that allows us to determine the diffusion length L of the Ge adatoms [14]. The fit reveals almost identical diffusion lengths of 5.0 ± 0.5 μm on the patterned and unpatterned areas.

We now consider the second island layer in Fig. 2(b). In this case, we also observe an island-free region. A simple exponential function is, however, not able to fit the evolution of Θ across the interface. The situation is complicated by the fact that the strain fields originating from buried islands significantly affect the Ge adatom diffusion and nucleation. We describe the distribution of Θ in a more general way using the error function $\mathrm{erf}[(x - x_0)/2L]$, where x_0 is the center of the fitting function. In this case, we find a significantly shorter diffusion length on the unpatterned area than on the patterned area. For 7 ML Ge in the second layer, we observe a slight volume overshoot on the flat surface near the island-free region [marked as "P" in Fig. 2(b)]. This effect cannot be explained assuming a simple diffusion theory.

In order to capture the physics of our experimental observations, we have developed a more quantitative growth model for a large surface area (80×80 μm^2). We consider the *mean-field* energy "felt" by the deposited Ge material. This total energy E is derived from the chemical potential for single Ge adatoms [5,15] and is defined as

$$E = E_b + E_{curv} + E_{str}, \tag{1}$$

where E_b is a binding energy on the planar substrate taken as a constant, E_{curv} is the mean-field energy contribution due to the surface curvature, and E_{str} is the strain energy contribution due to the buried islands.

In the case of the first island layer, there is no strain energy contribution ($E_{str} = 0$) to the total energy. Instead, the patterned area is exclusively characterized by surface curvature and can be taken as a sink for the deposited material, since the mean-field energy due to surface curvature is expected to be lower in this area than on the planar surface. The total energy prior to growth of the first island layer is shown in Fig. 3(a).

For the second layer, the surface is flat prior to island growth [16]. Hence, there is no contribution from the surface curvature to the total energy. The elastic strain

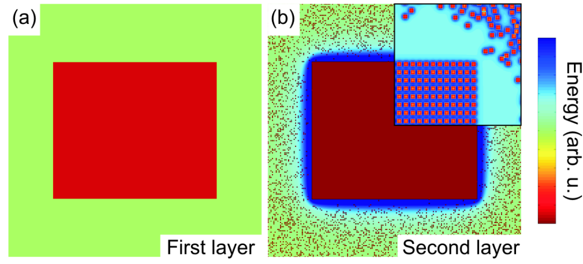

FIG. 3 (color online). (a) Total energy prior to first layer growth. The surface curvature lowers the total energy on the patterned area. (b) Total energy prior to second layer growth. The profile is characterized by short- and long-range strain contributions caused by buried islands in the first layer.

energy profile E_{str} is calculated using an analytical expression for a single island [17] and then by adding the strain contributions from all islands in the patterned area [7]. The buried Ge islands are treated as square-based boxes with 160 nm base length and 20 nm height. We take into account the size of the patterned area ($60 \times 50\ \mu m^2$), the mean island distance in the trenches (250 nm), and the trench period (320 nm) for the strain calculation. For simplicity, we assume a two-dimensional periodic array. Figure 3(b) shows the energy profile before deposition of the second island layer. The patterned area is on average tensile strained due to the buried ordered island array while the surrounding area is compressively strained. This compression will modify the diffusion of the Ge material around the patterned area. In addition, the short-range tensile strain outside the patterned area (small points), originating from the random buried islands, is magnified in the inset of Fig. 3(b).

On the long-range scale, the Ge material diffusion follows the gradient of the mean-field energy. For our simulation, we choose a domain discretized into an area of 300×300 pixels with periodic boundary conditions. At the center of this domain, an area of 120×100 is taken as the patterned area. In this model, the Ge material is placed inside the domain (deposition) and can subsequently diffuse (or stop) with a diffusion probability p_i. For an event i, the diffusion probability p_i is defined as the ratio between the diffusion flux of that event i to the total diffusion flux [18]. For an event i, the diffusion flux for the deposited Ge is given by [19]

$$F_i = F_0^{D,S} \exp(-\Delta E / k_B T), \qquad (2)$$

where E is defined in Eq. (1) and ΔE is the energy difference between two neighboring pixels. T is the substrate temperature, k_B is Boltzmann's constant, and $F_0^{D,S}$ is a constant. During diffusion, the Ge material can either stop at a pixel (in that case $F_0^{D,S} = F_0^S$) or diffuse to a neighboring pixel (in that case $F_0^{D,S} = F_0^D$). In our model, we decompose the strain energy originating from the buried islands into two terms, i.e., $E_{str} = E_{str}^L + E_{str}^S$, where E_{str}^L is the long-range strain energy and E_{str}^S is the short-range tensile strain energy contribution from the buried island array. E_{str}^L corresponds to a compressive strain energy $E_{str}^{L,U}$ outside the pattern, while inside the pattern it corresponds to a tensile strain energy $E_{str}^{L,P}$ [see Fig. 4(b)]. E_{str}^S is responsible for the vertical ordering in stacked island structures [9,20]. Hence, the E_{str}^S term increases the material accumulation probability on the pixel located directly above a buried island. For the second layer growth simulation, we define E_{str}^S as $\delta(x, y)\Delta E_{str}^S$, where $\delta(x, y) = 1$ directly above a buried island and zero elsewhere. ΔE_{str}^L is the amplitude of the long-range compressive strain, which repels Ge material diffusing towards the patterned area. Based on our considerations, we schematically plot the expected material distributions Θ and energy profiles E for the first and second island layers in Figs. 4(a) and 4(b).

Our growth simulation is carried out as follows: in each simulation step, the Ge material is randomly deposited onto one of the 300×300 pixels. Then, the material diffuses to a neighboring pixel according to the probability p_i, which depends on the flux defined in Eq. (2). The diffusion continues until nucleation occurs.

Figure 5 shows the material distributions obtained from averaging over 100 simulations. For the first island layer [Fig. 5(a)], a good description of our experiments can be obtained with $F_0^D = 400 \times F_0^S$ and $\Delta E_{curv} = 154$ meV. The ratio of F_0^D and F_0^S defines the average number of diffusion steps before Ge material stops. Taking $F_0^D = 400 \times F_0^S$ and assuming $\Delta E = 0$, we obtain a diffusion length of 8.1 μm on a flat surface. The two-dimensional simulation is shown in Fig. 5(a) and the material distribution along the solid line is rescaled in the y direction and plotted in Fig. 2(a) (open symbols) together with the experimental data. We obtain a good fit of the experimental results, confirming our assumption that on the long-range scale the patterned area can be considered as a material sink for the deposited Ge.

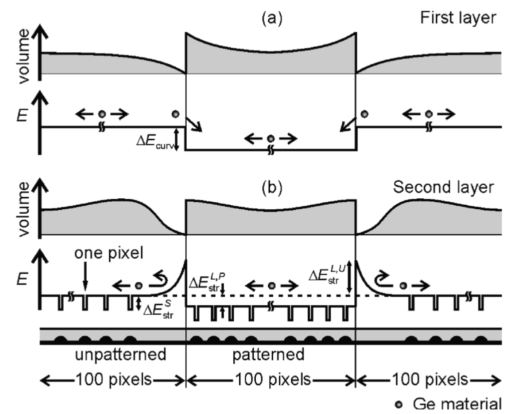

FIG. 4. Schematic illustration of the growth model for (a) the first and (b) the second layer. The upper part presents the expected volume profile of the deposited material while the lower part shows the assumed energy profile across the patterned area.

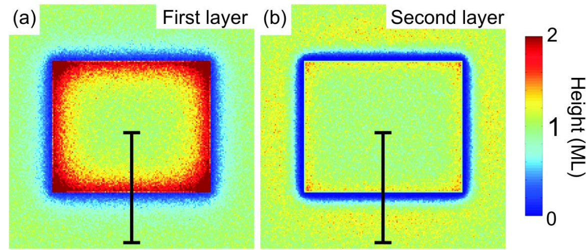

FIG. 5 (color online). Material distribution obtained from (a) first layer simulation and (b) second layer simulation. The volume along the solid lines is rescaled and plotted in Fig. 2.

For the second layer, the simulation result is shown in Fig. 5(b). We use the following parameters for this simulation: $F_0^D = 400 \times F_0^S$, $\Delta E_{\rm str}^S = 34$ meV, and $\Delta E_{\rm str}^{L,U} = 1.15$ eV. The value of $\Delta E_{\rm str}^S$ is compatible with our calculations of the strain energies found on top of the buried islands (18 meV). However, the fitted $\Delta E_{\rm str}^{L,U}$ is much larger than expected ($\sim$ meV). The reason for this apparent discrepancy lies in the lateral scaling of the model. In our simulation the Ge material needs less than ten diffusive steps to overcome the long-range barrier $\Delta E_{\rm str}^L$, while in reality a Ge adatom hops many thousand times to diffuse over this barrier. We determine the cross-sectional profile of the material distribution along the line indicated in Fig. 5(b). The rescaled results are shown as open symbols in Fig. 2(b). Our simulations can excellently fit the asymmetric material distribution across the interface between the patterned and the unpatterned area. The simulation can explain the material accumulation at position P in Fig. 2(b). The long-range compressive strain repels Ge material diffusing towards the patterned area thus leading to a material accumulation in the vicinity of the island-free region.

Finally, we discuss the limitations of our model. Compared to the considered growth area, we use a simulation domain of extremely low resolution (only 300×300 pixels), which means that an island has a lateral size of a single pixel. The low resolution of our growth simulation implies that we cannot predict any short-range effects such as the island density, their local size homogeneity, nor the properties of the single islands such as their size and shape. Moreover, we neglect the wetting layer and consider a maximum coverage of only 1 ML. These assumptions mean that the calculated material distribution needs to be upscaled in the y direction by a free but constant factor to fit our experimental results. We have tried to understand our experimental data by leaving the diffusion barrier E constant ($\Delta E = 0$) and changing the nucleation barrier (smaller in the patterned area and higher on planar surface), which is included in the term $F_0^{D,S}$. By doing so, we always found an asymmetric diffusion profile in the first layer, which is in contrast to our experimental results.

In conclusion, we investigated the distribution of material accommodated in self-assembled islands across the interface between patterned and unpatterned areas. Our measurements imply that a material depletion region around the finite sized patterned area occurs for single and twofold stacked island layers. Simulations suggest that for the first layer the patterned area acts as a material sink. For the stacked layer, a strain-modulated surface was taken into account to explain a highly asymmetric diffusion in and around the pattern. Our results provide a better understanding of self-assembled island growth on finite sized patterned areas, which is of fundamental importance for future high integration of novel single quantum dot devices.

We thank K. v. Klitzing for his continuous interest. The work was supported by the BMBF (03N8711).

*Electronic address: g.kar@fkf.mpg.de

[1] D. L. Klein *et al.*, Nature (London) **389**, 699 (1997); B. H. Choi *et al.*, Appl. Phys. Lett. **73**, 3129 (1998); P. Michler *et al.*, Science **290**, 2282 (2000); Z. Yuan *et al.*, Science **295**, 102 (2002); A. Zrenner *et al.*, Nature (London) **418**, 612 (2002).
[2] H. Heidemeyer, C. Müller, and O. G. Schmidt, J. Cryst. Growth **261**, 444 (2004); F. Nakajima, Y. Miyoshi, J. Motohisa, and T. Fukui, Appl. Phys. Lett. **83**, 2680 (2003); Y. Nakamura *et al.*, Phys. Status Solidi B **238**, 237 (2003).
[3] M. H. Baier, S. Watanabe, E. Pelucchi, and E. Kapon, Appl. Phys. Lett. **84**, 1943 (2004); S. Watanabe *et al.*, *ibid.* **84**, 2907 (2004).
[4] G. Jin *et al.*, Appl. Phys. Lett. **75**, 2752 (2003); K. C. Rajkumar *et al.*, *ibid.* **63**, 2905 (1993).
[5] B. Yang, F. Liu, and M. G. Lagally, Phys. Rev. Lett. **92**, 025502 (2004).
[6] O. G. Schmidt *et al.*, Appl. Phys. Lett. **77**, 4139 (2000).
[7] H. Heidemeyer, U. Denker, C. Müller, and O. G. Schmidt, Phys. Rev. Lett. **91**, 196103 (2003).
[8] Z. Zhong, and G. Bauer, Appl. Phys. Lett. **84**, 1922 (2004); S. Kiravittaya, H. Heidemeyer, and O. G. Schmidt, Physica (Amsterdam) **23E**, 253 (2004).
[9] O. Kienzle *et al.*, Appl. Phys. Lett. **74**, 269 (1999).
[10] We assume a constant wetting layer thickness.
[11] Z. Zhong *et al.*, J. Appl. Phys. **93**, 6258 (2003).
[12] G. Medeiros-Ribeiro *et al.*, Science **279**, 353 (1998).
[13] F. M. Ross, R. M. Tromp, and M. C. Reuter, Science **286**, 1931 (1999).
[14] A. Hartmann *et al.*, J. Appl. Phys. **77**, 1959 (1995).
[15] Q. Xie *et al.*, Phys. Rev. Lett. **75**, 2542 (1995).
[16] A more detailed study will be published elsewhere.
[17] J. Zhang, K. Zhang, and J. Zhong, Appl. Phys. Lett. **84**, 1853 (2004).
[18] The total diffusion flux is the summation of the different fluxes from all possible events (diffusion or stop) for the considered pixel.
[19] This equation is derived from atomistic considerations of adatom diffusion. A more detailed calculation will be published elsewhere.
[20] J. Tersoff, C. Teichert, and M. G. Lagally, Phys. Rev. Lett. **76**, 1675 (1996).